

NZ.
First Quarterly Report
for

SOLAR CELL COVER GLASS DEVELOPMENT

(15 June 1966 through 1 September 1966)

Contract Number: NAS5-10236

Prepared by:

Ion Physics Corporation
Burlington, Massachusetts

Prepared for:

Goddard Space Flight Center
Greenbelt, Maryland

FACILITY FORM 502	N67-26177	
	(ACCESSION NUMBER)	(THRU)
	38	1
	(PAGES)	(CODE)
	0084005	18
	(NASA CR OR TMX OR AD NUMBER)	(CATEGORY)

ION PHYSICS CORPORATION



A Subsidiary of High Voltage Engineering Corporation

BURLINGTON, MASSACHUSETTS

Quarterly Technical Progress Report No. 1

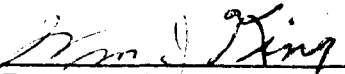
15 June 1966 through 1 September 1966

SOLAR CELL COVER GLASS DEVELOPMENT

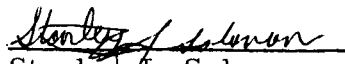
National Aeronautics and Space Administration
Goddard Space Flight Center
Greenbelt, Maryland

Contract NAS5-10236

Project Manager:


Dr. William J. King

Project Engineer:


Stanley J. Solomon

ION PHYSICS CORPORATION
BURLINGTON, MASSACHUSETTS

PRECEDING PAGE BLANK NOT FILMED.
CONFERENCES

A conference was held at Ion Physics Corporation on 21 June 1966 at which Mr. W. Cherry discussed program objectives with IPC personnel.

OBJECTIVE

The objective of this program is refinement and economic optimization of techniques for fabrication of thick integral coverslips for silicon solar cells. An a priori assumption is that integral coverslip cells must show a definite superiority over conventional glued coverslip cells. The consequences of this assumption provide natural guidelines for selection of candidate coverslip materials, possible fabrication techniques and environmental test end points. Specifically, all coverslip materials that are known to significantly degrade under UV, proton or electron irradiation must be categorically excluded from consideration. Similarly, all fabrication techniques that are inherently deleterious to the cell structure itself must be rejected. Finally, the environmental and radiation test end points must be at least as severe as those encountered with glued coverslip cells. For ease in comparison, final testing is to be done on cells with 6 mil integral coverslips.

SUMMARY

IPC's proprietary high vacuum sputtering process has been shown to be well suited to the deposition of integral SiO_2 coverslips onto silicon solar cells. Since, however, this process has a rate limitation, it is important to examine other processes that could more quickly deposit SiO_2 over an initial high vacuum sputtered layer. Both reactive sputtering and electron beam evaporation have been investigated as a means of rapidly building up coverslip thickness.

While the work to date has been of satisfactory quality, its quantity has been below expectation, forcing a three-month slippage of first quarter goals. This situation has resulted from slow delivery of both the electron beam gun for evaluation of evaporated SiO_2 and the large diameter Si target for use in the next phase of the reactive sputtering studies. Gun delivery is now promised for the end of September. The Si target should be available during the first week of October.

The intermediate sized high vacuum sputtering apparatus has been used for fabrication of integral coverslips up to 3 mils thick. The source of the granularity problems observed in reactive sputtering has been tentatively identified and should be eliminated with a new geometric arrangement. Thin optically clear films of MgO and Al_2O_3 have been deposited by high vacuum reactive sputtering. Silicon nitride films formed in the same way have been brownish. Thin optically clear lead glass films have also been deposited by high vacuum sputtering.

TABLE OF CONTENTS

	<u>Page</u>
CONFERENCES	iii
OBJECTIVE	iv
SUMMARY	v
1. PROGRAM CONSIDERATIONS	1
1.1 Background	1
1.2 Approach	1
1.3 Coverslip Materials	7
1.4 Temperature Effects	9
1.5 Anti-Reflection Coatings	14
2. EXPERIMENTAL RESULTS	15
2.1 Deposition Techniques	15
2.1.1 Reactive Sputtering	15
2.1.2 Electron Beam Evaporation	17
2.2 Other Materials	17
2.3 Thermal Cycling	18
2.4 UV and Vacuum Testing	18
2.5 Radiation Testing	21
3. FUTURE PLANS	23
4. REFERENCES	25

LIST OF ILLUSTRATIONS

<u>Figure</u>		<u>Page</u>
1	Thermal Expansion vs Temperature	8
2	Sandwich Structure	11
3	Dependence of θ on ΔL	13
4	Thermal Cycle Test	19

LIST OF TABLES

<u>Table</u>		<u>Page</u>
I	UV Degradation of Coverslip Adhesives	2
II	UV Degradation of UV Reflective Filters Deposited on Corning 7940 Fused Silica	3
III	Electron and Proton Degradation of Solar Cell Adhesives and Filters	4
IV	Electron Degradation of Coverslip Materials	5
V	Proton Degradation of Coverslip Materials	6
VI	Environmental Test Specifications	20

1. PROGRAM CONSIDERATIONS

1.1 Background

Coverslips are required to protect solar cells from displacement-producing space radiations. While the types of radiation, and their intensities and energies, vary widely in space, they are sufficiently well charted to allow prediction of the fluxes encountered in any particular mission, thus allowing calculation of the required coverslip thickness. Since the presence of coverslips reduces power-to-weight ratios, it is desirable to use minimum thickness slips. This latter consideration necessitates a trade-off between maximum cell protection and minimum coverslip weight. From a practical standpoint, slips thinner than 6 mil cannot be economically applied. For many missions, however, 1 mil coverslips are sufficient. Since integral coverslips are, by nature, built-up, an integral coverslip technique would allow use of thin slips, where sufficient, as well as thick slips.

A second major advantage of an integral coverslip is the absence of materials that degrade under UV and radiation exposure. In conventionally slipped cells, organic adhesives are used to attach the slips. Since these compounds darken under UV exposure (Table I), they must be protected by UV filters that themselves darken under UV exposure (Table II). Moreover, both the filter and adhesive darken under electron and proton bombardment (Table III). A subsidiary advantage of integral coverslipped cells is that the absence of organic adhesives allows the cells to be heated to 400 to 450°C for radiation damage annealing. The final, although not necessarily the least important advantage of integral coverslips is the expectation that the slipping technique would also insulate and stabilize cell edges.

1.2 Approach

Radiation tests have indicated that only certain glasses (SiO_2 , Al_2O_3 and lead glass) do not darken under simulated space electron and proton fluxes (see Tables IV and V). While MgO and Si_3N_4 have not been adequately tested, radiation darkening has ruled out the use of low temperature softening glasses that could be flowed over the cell surface. (Additionally, flowing of these glasses requires temperatures that are deleterious to the cell itself and incompatible with normal Ti-Ag contacts.)

Of the three acceptable materials, SiO_2 is by far the most thoroughly investigated. Moreover, Al_2O_3 , MgO and lead glasses had not previously been deposited by low temperature techniques. While the literature suggests a wide variety of techniques for obtaining SiO_2 films on Si, they all have the common feature that the films spontaneously strip when their thickness approaches $20 \times 10^3 \text{ \AA}$. In contrast to this behavior, SiO_2 films deposited on Si by the IPC developed high vacuum sputtering technique do not split at $20 \times 10^3 \text{ \AA}$, 1 mil or any thickness yet attained, even under rapid thermal cycling between -195°C and

Table I
UV Degradation of Coverslip Adhesives

Adhesives	Sun-Hours Exposure	% Change in Transmission at Wavelength					Reference
		0. 5 μ	0. 6 μ	0. 7 μ	0. 8 μ	0. 5-0. 9 μ	
ES-10 (Spectrolab)	630	23	13	8. 6	6. 4	-	1
15-E (Furane)	630	43	31	27	25	-	1
XR63488 (Dow)	500	-	-	-	-	0	2
XR63488	2000	-	-	-	-	0	2
XR63488 + Primer	500	-	-	-	-	1. 1	2
XR63488 + Primer	2000	-	-	-	-	1. 2	2
LTV-602 (GE)	500	-	-	-	-	1. 1	2
LTV-602	2000	-	-	-	-	0. 6	2
LTV-602 + Primer	500	-	-	-	-	0. 6	2
LTV-602 + Primer	2000	-	-	-	-	2. 9	2

Reference 1: Campbell, F. J., "Effects of Radiation on Transmittance of Glasses and Adhesives", Proceedings of the Seventeenth Annual Power Sources Conference (May 1963).

Adhesive samples were cast as 1 to 2 mil films between 30 mil fused silica bases and 6 mil fused silica cover sheets that did not have UV filters.

Reference 2: "Campbell, F. J., "Status of Solar Cell Cover Material Radiation Damage", Proceedings of the Fifth Photovoltaic Specialists Conference (October 1965).

Adhesive samples were ~ 1 mil films between Corning 7940 bases and "blue" filtered Corning 7940 cover sheets.

Table II
UV Degradation of UV Reflective Filters Deposited on
Corning 7940 Fused Silica

Filter	Ultraviolet Exposure, Sun-Hours	Average Initial Transmittance % (500-1100 mμ)	Average Final Transmittance % (500-1100 mμ)	Average Change in Transmittance % (500-1100 mμ)
none	703	93.3	92.0	-1.4
"blue-red"	590	93.3	87.3	-6.4
"blue"	735	93.0	91.0	-2.2

From: Campbell, F. J., "Status of Solar Cell Cover Material Radiation Damage", Proceedings of the Fifth Photovoltaic Specialists Conference (October 1965).

Table III
Electron and Proton Degradation of Solar Cell
Adhesives and Filters

Material Description	% Change in Transmittance at Wavelengths		
	0.5 μ	0.6 μ	0.7 μ
A. 1 Mev Electrons - Total Dose of 10^{16} e-cm ⁻²			
(1) Microsheet (6 mil) Corning 0211	5.6	3.3	2.2
(2) Same as (1) + A-R coating + "blue" filter	7.3	5.1	4.2
(3) Same as (1) + A-R coating + "blue-red" filter	9.9	8.6	6.9
(4) 3-mil microsheet + A-R coating + "blue" filter	3.7	2.1	
(5) Fused silica (66 mil) Corning 7940	1.7	2.2	1.1
(6) Fused silica-Corning 7940 (20 mil) + A-R coating + "blue" filter	1.1	2.2	1.1
(7) Adhesive ES-10 (Spectrolab)	1.7	1.7	1.1
(8) Adhesive 15-E (Furane)	24	13	12
(9) Adhesive DER-332 (LC) (Dow)	8.6	9.1	4.5
B. 4.6 Mev Protons - Total Dose of 4×10^{11} p-cm ⁻²			
(1) Microsheet (6 mil) Corning 0211	3.4	1.1	1.1
(2) Same as (1) + A-R coating + "blue" filter	5.2	2.1	1.1

From: Campbell, F. J., "Effects of Radiation on Transmittance of Glasses and Adhesives", Proceedings of the Seventeenth Annual Power Sources Conference (May 1963).

Table IV
Electron Degradation of Coverslip Materials

	Manufacturer	Material	Thickness (Inches)	Energy (Mev)	Dose (e-cm ⁻²)	% Change in Transmission 0.4-1.2μ
Al ₂ O ₃	Linde Company	Sapphire	0.080	1.2	2.7 x 10 ¹⁵	0
	Linde Company	Sapphire	0.120	1.2	1 x 10 ¹⁷	0
	Linde Company	Sapphire	0.040	0.3	2.7 x 10 ¹⁵	0
Synthetic Fused Silica	Engelhard	Suprasil II	0.0625	1.2	2.7 x 10 ¹⁵	0
	Corning	# 7940 UV Grade	0.125	1.2	2.7 x 10 ¹⁵	0
	Corning	# 7940 Optical Grade	0.125	1.2	2.7 x 10 ¹⁵	0
	Corning	# 7940 Optical Grade	0.250	1.2	1 x 10 ¹⁷	2.2
	Thermal American	Spectrosil A	0.125	1.2	2.7 x 10 ¹⁵	0
	Thermal American	Spectrosil B	0.0637	1.2	2.7 x 10 ¹⁵	0
	Dynasil Corporation	Optical Grade	0.125	1.2	2.7 x 10 ¹⁵	0
	Dynasil Corporation	Optical Grade	0.125	1.2	1 x 10 ¹⁷	1.5
	Dynasil Corporation	Optical Grade	0.125	0.30	2.7 x 10 ¹⁵	0
Fused Quartz	Engelhard	Optical Grade	0.0625	1.2	2.7 x 10 ¹⁵	1.8
	Engelhard	Homosil	0.0625	1.2	2.7 x 10 ¹⁵	2.1
	Engelhard	Ultrasil	0.0625	1.2	2.7 x 10 ¹⁵	6.43
	Engelhard	Infrasil	0.0625	1.2	2.7 x 10 ¹⁵	23.4
	General Electric	# 104	0.0935	1.2	2.7 x 10 ¹⁵	0.8
	General Electric	# 104	0.0935	0.30	2.7 x 10 ¹⁵	1.1
	General Electric	# 105	0.0935	1.2	2.7 x 10 ¹⁵	30.0
	General Electric	# 105	0.0935	0.30	2.7 x 10 ¹⁵	5.3
	General Electric	# 106	0.0935	1.2	2.7 x 10 ¹⁵	28.6
	General Electric	# 106	0.0935	0.30	2.7 x 10 ¹⁵	5.3
	Corning	Vycor (# 1913)	0.250	1.2	1.69 x 10 ¹⁵	58.9
	Corning	Crystal Quartz	0.292	1.2	2.7 x 10 ¹⁵	26.8
Special Glasses	Corning	# 8362	0.0625	1.2	2.7 x 10 ¹⁵	2.4
	Corning	# 8363	0.0625	1.2	2.7 x 10 ¹⁵	0
	Corning	# 8365	0.0625	1.2	2.7 x 10 ¹⁵	0
	Corning	Microsheet (# 0211)	0.006	1.2	2.7 x 10 ¹⁵	1.8
	Corning	Microsheet (# 0211)	0.026	1.2	2.7 x 10 ¹⁵	7.6
	Corning	Microsheet (# 0211)	0.026	1.2	1 x 10 ¹⁷	12.2
Common Glasses	Pittsburgh	Solex	0.250	1.2	2.7 x 10 ¹⁵	2.7
	Pittsburgh	Plate Glass	0.250	1.2	1.69 x 10 ¹⁵	26.0
	Blue Ridge	Feurex	0.250	1.2	2.7 x 10 ¹⁵	25.2

From: Haynes, G. A. and Miller, W. E., "Effects of 1.2 and 0.3 Mev Electrons on the Optical Transmission Properties of Several Transparent Materials", NASA Technical Note D-2620.

Table V
Proton Degradation of Coverslip Materials

Manufacturer	Material	Thickness (Inches)	Energy (Mev)	Dose (p-cm ⁻²)	% Change in Transmission at Wavelength		
					0.5μ	0.6μ	0.7μ
Corning	Microsheet (# 0211)	0.006	4.6	4 x 10 ¹¹	3.4	1.1	1.1
Corning	Microsheet (# 0211) + A-R coating + "blue" filter	0.006+	4.6	4 x 10 ¹¹	5.2	2.1	1.1
Corning	Fused Silica (# 7940)	0.030	4.6	4 x 10 ¹¹	0	0	0
Corning	Fused Silica (# 7940) + A-R coating + "blue" filter	0.020	4.6	4 x 10 ¹¹	0	0	0

From: Campbell, F. J., "Effects of Radiation on Transmittance of Glasses and Adhesives",
Proceedings of the Seventeenth Annual Power Sources Conference (May 1963).

200°C. This technique forms the basis for fabrication of integral coverslip cells.

Although high vacuum sputtered SiO_2 gives fully acceptable integral coverslips, this process appears to be economically attractive only up to 3 mil thick slips. For thicker slips, a faster deposition technique used in conjunction with high vacuum sputtering is desirable. Literature references indicate that reactive sputtering and electron beam evaporation give higher deposition rates than competing processes. Moreover, neither of these techniques inherently requires a significant increase in cell temperature during deposition.

1.3 Coverslip Materials

Tables IV and V summarize the effects of electrons and protons on a variety of candidate coverslip materials. Of particular note is the fact that fused silica, sapphire and lead glass do not darken while all other materials are more or less damaged. In addition to these three materials, MgO and Si_3N_4 are also worthy of consideration. Unfortunately there is only neutron damage optical data available for MgO and essentially no data for Si_3N_4 .

While all of these five, except lead glass, can be deposited by high vacuum sputtering, reactive sputtering and electron beam evaporation, it remains to determine which is the most suitable candidate for a coverslip material. In addition to being readily depositable and not darkening under radiation, the coverslip material should have an expansion coefficient near that of silicon. Thermal expansion curves for Si , SiO_2 , Al_2O_3 , MgO , Si_3N_4 and CeO_2 are grouped in Figure 1 along with single value data for the lead glasses. The data for Al_2O_3 and Si_3N_4 is particularly suspect. The Al_2O_3 data is derived from many different determinations on high alumina ceramics and crystalline aluminas. The Si_3N_4 data is from measurements on bulk crystalline Si_3N_4 . As a consequence, expansion coefficients for amorphous films of these materials, and perhaps MgO also, may be moderately different.

As will be analyzed in more detail in Section 1.4, it is desirable to minimize thermal expansion mismatches between the Si cell and coverslip. Proceeding from this basis, the use of MgO does not appear attractive. Al_2O_3 is a much better match to Si and might be acceptable. It does, however, have the disadvantage that, if deposited slightly above room temperature, the top Al_2O_3 surface would be in tension at room temperature, and thus more susceptible to cracking. The magnitude of this potential problem must be determined by experiment. Both Si_3N_4 and SiO_2 have a smaller expansion coefficient than Si and hence, by analogy, will give films whose top surface is in compression, thus minimizing potential surface cracking. The thermal expansion mismatch between SiO_2 and Si is fairly large but is not too bad between -100 and +100°C. It would appear that Si_3N_4 is at least as good a match to Si as is SiO_2 and might be slightly superior. While the change of thermal expansion coefficient in going from crystalline Si_3N_4 to amorphous Si_3N_4 cannot be evaluated, the reported cracking of thick amorphous Si_3N_4 films deposited on Si is rather discouraging.

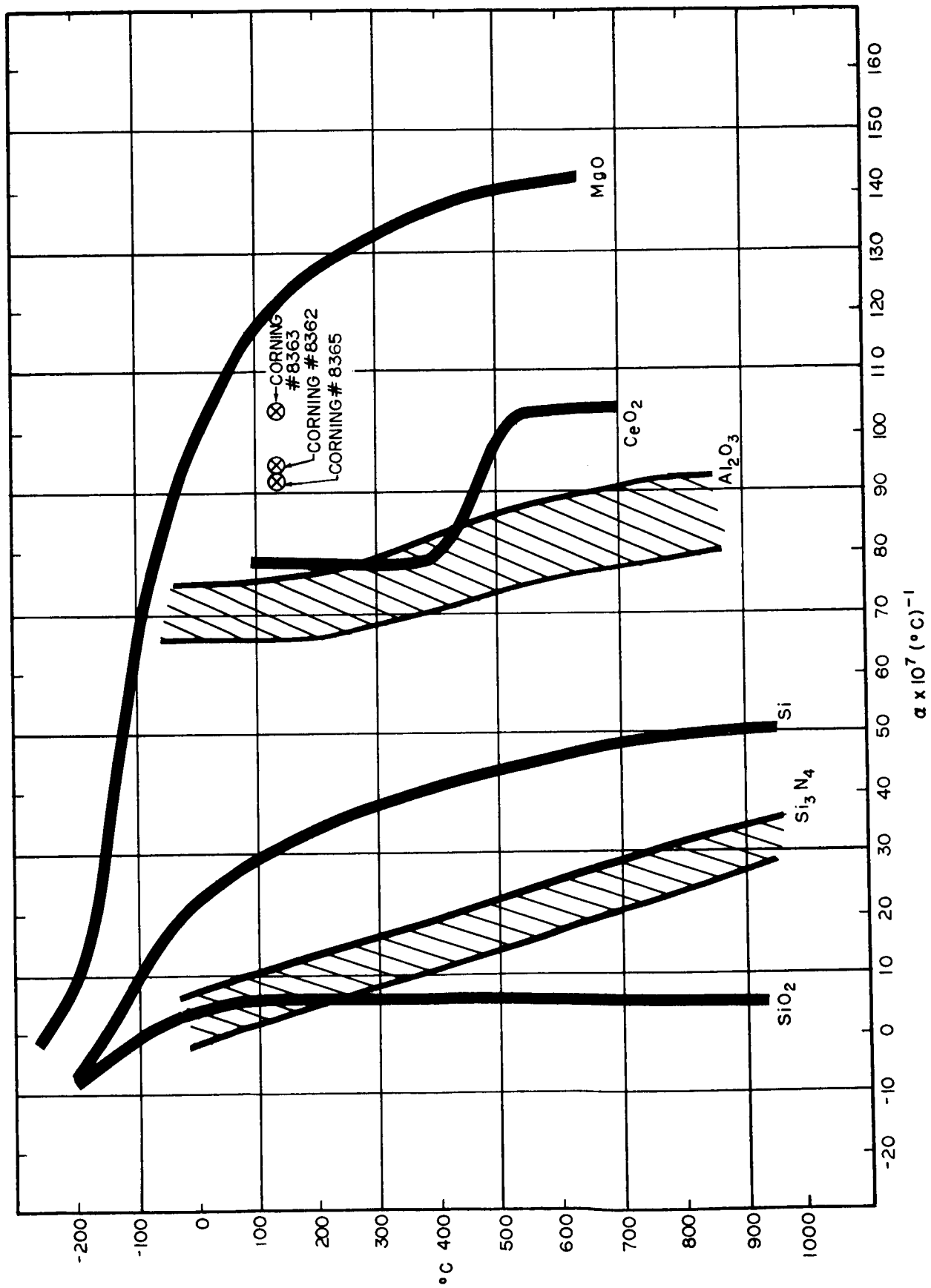


Figure 1. Thermal Expansion vs Temperature

These latter observations may, however, be caused by the high temperature deposition techniques that were used. While only single point data is available for the lead glasses, their expansion coefficients appear to be too large.

Since none of the single component systems are really good expansion matches to Si, two component systems, consisting of a high expansion and a low expansion material, are superficially appealing. The only real possibility, however, is a MgO-SiO₂ mixture. Si₃N₄ is unstable with respect to SiO₂ and hence, when deposited with Al₂O₃ or MgO, would give a non-stoichiometric Si₃N₄ that contained an appreciable amount of SiO₂ and a non-stoichiometric Al₂O₃ or MgO. Little is known about the properties of mixtures of these compounds except that the presence of Al in the SiO₂ system is the principle cause of SiO₂ radiation darkening. Since Na does not appear to produce radiation darkening in SiO₂, Mg might be expected to be inactive also. Even with a MgO-Si₃N₄ system, there is still a deposition problem since the mixture certainly could not be produced by reactive sputtering and probably not by evaporation. While high vacuum sputtering is applicable, the highly desirable increased deposition rate could not be obtained. Because of the effect of Al on SiO₂ radiation darkening, an Al₂O₃-SiO₂ system could not be considered. As previously noted, a MgO-SiO₂ system (Forsterite) might be acceptable. This system could be deposited by all three deposition techniques. Its behavior under radiation is unknown. It should be noted that Si₃N₄-SiO₂ systems have been deposited on Si. The properties of this system are also unknown and its utility for the present application is doubtful.

From the preceding discussion and the general state-of-the-art, it is most logical to start the integral coverslip work with SiO₂. Al₂O₃ would have to be considered the first alternate material because its radiation behavior is well known. The third choice, Si₃N₄, may turn out to be the best expansion match, but its properties under radiation must be determined first.

1.4 Temperature Effects

There are two types of temperature effects that are of interest in integral coverslip development. The first is a processing temperature limitation that is imposed by the cell construction itself and affects only the choice of possible coverslip deposition techniques. Specifically, the low ohmic contact resistance and bonding properties of the normal Ti-Ag contact fingers are seriously degraded if contacted cells are reheated to temperatures above 500°C. While Ti-Ag contacts are known to be wanting in many respects, it is not reasonable that they should be rejected solely to allow integral coverslips. Moreover, heating Si to temperatures above 600°C, even under "clean" conditions, that would be very difficult to obtain when coating a finished cell, can produce significant lifetime degradation and hence reduce the conversion efficiency of the cell.

The effect of these two process temperature limitations is only that of eliminating certain possible deposition techniques that would have had to be

eliminated for other reasons in any case. For example, the glass compositions that could be applied as frits and fired, all darken under electron irradiation. While SiO_2 and Al_2O_3 do not darken, they will not flow and fuse below the melting point of Si. Growth kinetics prohibit the attainment of grown SiO_2 films as thick as 0.5 mil and pyrolytic decomposition processes are reportedly incapable of producing continuous adherent SiO_2 (or Si_3N_4) coatings more than 2 to 4 microns thick. By contrast, none of the three deposition processes under consideration require elevated deposition temperatures and both electron beam evaporation and reactive sputtering have higher deposition rates than any of the competing processes except frit fusing.

The second temperature effect, inherent to all integral coverslip systems, is based on the unequal thermal expansions of the Si cell and coverslip (see Figure 1). Ignoring, for the moment, all questions of stress in the cell coating, it is readily seen that integral coverslipped cells will be flat only at the temperature at which the slip was deposited and curved at all other temperatures. For SiO_2 , cells will be convex (upward) at temperatures below the deposition temperature and concave (upward) at higher temperatures. Since the cells are at room temperature during testing and mounting, it is most convenient to choose a low deposition temperature so that the cells are flat at room temperature. The curvature at other temperatures must then be accounted for in the cell mounting technique. It is also necessary to examine the stresses in the various layers of an integral cell. Consider a two-layer sandwich of materials having expansion coefficients C_a and C_b (see Figure 2). Initially, when the two layers are bonded together, they are the same length. The temperature is then changed at ΔT . Each material, if not restrained, would try to change its length by $\Delta L_a = C_a L_1 \Delta T$ and $\Delta L_b = C_b L_1 \Delta T$. In the expanded (or contracted) condition the lengths differ by $(L_1 + \Delta L_a) - (L_1 + \Delta L_b) = \Delta L_a - \Delta L_b = \Delta L = (C_a - C_b) L_1 \Delta T$. The internal forces involved in preventing this length difference at the interface, assuming momentarily no relief by bending, are proportional to:

$$\frac{\Delta L}{L} = (C_a - C_b) \Delta T \quad (1)$$

and inversely proportional to the reciprocal sum of the compressive-extensional spring constants of the two layers. These spring constants are simply $K_a = E_a A_a / L_1$ lb/inch, where E_a is Young's modulus for material "A" and $A_a = wt_a$ is its cross-sectional area. The forces are then:

$$\begin{aligned} F &= K \Delta L \\ &= \Delta L \frac{1}{\frac{1}{K_a} + \frac{1}{K_b}} \end{aligned} \quad (2)$$

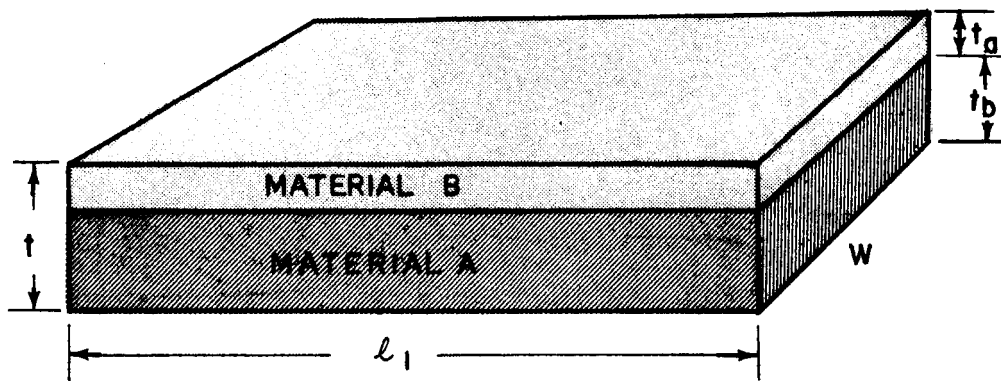


Figure 2. Sandwich Structure

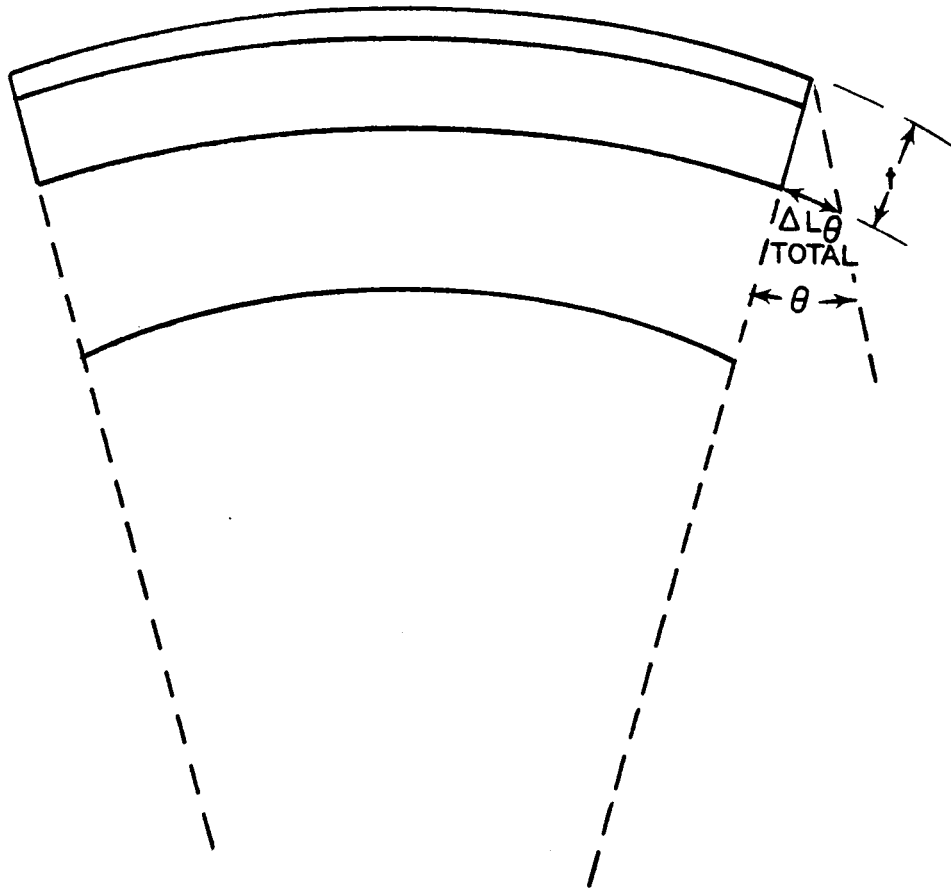
$$\begin{aligned}
F_a &= -F_b \\
&= \frac{\Delta L}{\frac{L_1}{E_a A_a} + \frac{L_1}{E_b A_b}} \\
&= \frac{(C_a - C_b) \Delta T L_1}{\frac{L_1}{E_a A_a} + \frac{L_1}{E_b A_b}} \quad (3) \\
&= \frac{(C_a - C_b) \Delta T}{\frac{1}{E_a A_a} + \frac{1}{E_b A_b}}
\end{aligned}$$

and the internal stresses are $B_a = F_a/A_a$ and $B_b = -F_a/A_b$. The above description is accurate if: (1) neither layer is thick enough for significant stress relief, implying the assumption of uniform strain throughout its thickness; (2) that significant stress relief has not occurred by bending, implying it has bent through an angle which is small compared to $\theta = \sin^{-1} 2 \Delta L/t$ (see Figure 3).

The above description is qualitatively correct at the interface even when condition (2) is violated. When there is significant bending, F is determined by substituting $\Delta L - (t/2 \sin \theta)$ for ΔL in Equations (2) and (3).

Assuming the interfacial bond to be adequate, breakage of one layer or the other will occur when B exceeds the yield strength of that material. The interfacial bond is in essentially pure shear. When the shear stress $S = F/L_1 W$ is greater than the shear strength, the interfacial bond will fail.

In practice, the Si-SiO₂ interface sandwiches an anti-reflective CeO₂ layer about 600 Å thick. IPC believes that although this layer adds an extra interface which could be a potential failure point, the shear strength of the intermediate material will always be greater than the interfacial shear strength. It is furthermore believed that the forces resulting from the thermal stressing of this layer itself will be a negligible effect on the overall force picture. This is due to the relatively small cross-sectional area of this layer. The anti-reflective coating is $(600 \text{ Å}/3,000,000 \text{ Å}) = 0.0002 = 0.02\%$ of the thickness of the cell. Considering the layer as one of a two-layer device, it can be seen that Equation (3) goes to zero as $A_a = Wt_a$ approaches zero and so the forces due to a 600 Å layer are essentially zero. This is not to say the layer will not itself be stressed to a level near or above its bulk yield point. But if this has happened, it has not produced an observable effect in IPC integral cover cells.



For small θ :

$$\Delta L_{\theta \text{ tot}} = t \tan \theta$$

$$\Delta L_{\theta} = \text{avg } \Delta L = \frac{t}{2} \tan \theta$$

Figure 3. Dependence of θ on ΔL

Calculations based on the foregoing are, of course, limited by the validity of the assumptions and of the data. IPC has not demonstrated that the thermal expansion coefficient, Young's modulus, or tensile strength of the sputtered SiO_2 layer is equivalent to that of fused silica. Further, numerical value of the tensile strength of the single crystal silicon is not reliable because of the variability of crystalline perfection upon which it depends. As a consequence, it appears to be inappropriate, at this time, to carry these calculations further.

1.5 Anti-Reflection Coatings

In addition to conversion losses that occur in the semiconductor itself, reflections at solar cell interfaces decrease the intensity of the incident light. For a SiO_2 coverslip on a Si cell, $\sim 3\%$ of the light is reflected at the air- SiO_2 interface and $\sim 30\%$ at the SiO_2 -Si interface. To reduce the latter loss, most cells are anti-reflected with an evaporated layer of SiO. While SiO has the proper refractive index ($n = 1.9$) to grade between Si and air, its index is too low to efficiently grade between Si and SiO_2 . IPC has developed a CeO_2 layer ($n = 2.35$) that gives a more efficient index gradient between Si and SiO_2 .

Neglecting, for the present, the design of anti-reflection coatings, it is appropriate to examine the physical and chemical properties of CeO_2 with respect to its appropriateness as an anti-reflection layer. CeO_2 is a low vapor pressure refractory oxide that is transparent in the 4 to $12 \times 10^3 \text{ \AA}$ region. While it is susceptible to reaction and O loss at high temperatures, IPC has found no evidence of instability in properly applied CeO_2 layers. It is interesting to note that O deficient CeO_2 is an n-type semiconductor. Hence, when applied to the surface of n-on-p cells, a thin layer of O deficient CeO_2 might act as a reasonably conductive transparent front contact. However, the refractive index of CeO_2 falls rapidly with O deficiency, thus neutralizing any gain that might be achieved from a transparent contact. CeO_2 is commonly added to various glasses for a variety of reasons that range from producing opacity to inhibiting solarization. In each of these cases, however, CeO_2 reacts with specific constituents of the glass to produce the desired effect. With a pure SiO_2 glass, there should be no effect due to the presence of CeO_2 . Experimentally, IPC has found no chemical effect or proton damage darkening in integral coverslip cells anti-reflected with CeO_2 . In summary, CeO_2 has the proper refractive index for grading between Si and SiO_2 and no demonstrated disadvantages.

2. EXPERIMENTAL RESULTS

2.1 Deposition Techniques

It is important to reiterate that SiO₂ integral coverslips deposited by high vacuum sputtering have already demonstrated their ability to satisfy most of the requirements of this contract. The high vacuum sputtering process is economically attractive for deposition of thin slips on a volume basis. Limited deposition rates coupled with fluctuating use factors on a relatively expensive equipment suggest that high vacuum sputtering would not, in general, be economically attractive for thick slips.

While the rate limitation is not absolute, the physics of the deposition process is such that equipment costs for a high current density (high deposition rate) apparatus are very much higher than for a low current density large area apparatus. Consequently, the production high vacuum sputtering equipment that is currently being built by IPC is designed to simultaneously coat thousands of cells at relatively low deposition rates. Since the demand for thick slips is highly variable, additional high vacuum sputtering systems required to handle this demand could not be efficiently scheduled thus increasing coverslipping costs per mil of SiO₂ by a factor of 4 to 6. The desirability of developing faster deposition systems for building-up coverslip thickness is evident from these economic considerations.

Since the basic problem in fabricating integral coverslips, that of obtaining satisfactory Si-SiO₂ bonding, is solved by high vacuum sputtering, the requirements on the building-up process are less severe and allow solutions that are not admissible alone. In particular, the building-up process need only insure good SiO₂-SiO₂ bonding, which would be expected of any process, and not require high temperature processing steps. Reactive sputtering and electron beam evaporation satisfy both of these requirements while promising greater deposition rates than competing processes.

2.1.1 Reactive Sputtering

Of the various known SiO₂ deposition techniques, reactive sputtering and electron beam evaporation have the highest deposition rates. The latter process is discussed in the next section. In reactive sputtering, the parent metal of the compound that is to be formed is sputtered in the presence of a gas that forms the anionic component of the compound rather than in pure air as in normal sputtering. The sputtering rate is then that of the metal rather than that of the dielectric compound. Moreover, reactive sputtering is a dc process and hence, much more economic than the RF sputtering system needed for direct sputtering of dielectrics. Unoptimized SiO₂ deposition rates of 16×10^3 Å/hr have been reported.^(1,2) (IPC has observed partially optimized rates of 25×10^3 Å/hr.)

Reactive sputtering of SiO_2 was being investigated at IPC when this contract was received. The level of these efforts has subsequently been increased. Initial experiments were performed in a small bell jar vacuum system with an ~ 1.5 inch diameter Si target. The substrates were suspended at a variable distance above the target and connected to ground, while the target was connected to the negative terminal of an unfiltered dc supply capable of delivering 1 amp at 5000 volts. In general, this system produced good SiO_2 films that exhibited no absorption in the visible region. Because of the large power dissipation at the cathode (target) and the close target-substrate spacing, the substrates came to $\sim 300^\circ\text{C}$ during deposition.

Attempts to attach the substrates to a simple water cooled plate were not successful and the geometric arrangement was changed. Unfortunately a large number of other changes were made at the same time. In the new geometry the target was suspended above a grounded water cooled metal plate that supported the substrates. In this arrangement, substrate temperatures increased only to $\sim 150^\circ\text{C}$. The Si target was changed to an assembly of four rectangular bars that were supported on a sand-finish quartz plate that had a $3\text{-}3/4$ inch² cut-out in the center. This plate was spaced from the anode by quartz bars. Films deposited from this arrangement have exhibited a granular structure that gives rise to diffuse scattering. The absorption spectra of these films shows the optical density increase with decreasing wavelength that is characteristic of Rayleigh scattering, suggesting the diffuseness is due to scattering by small included granules.

No variation of operating voltage, pressure or gas composition, including traps to eliminate water vapor, appreciably reduced the diffuseness of the films. Within the last month, the source of the problem has tentatively been identified as coming from both the quartz supporting structure and the Si bars. This observation was quite unexpected and cannot really be explained. It has, however, been observed that partial elimination of these quartz supports and use of a single Si bar results in clearer films.

Since, in the present geometry, some type of dielectric support is needed for the Si target, a new setup is being constructed. This arrangement will use a large (6 inch diameter) Si target as the top plate on a short section of Pyrex pipe that rests on the bell jar baseplate. As the anode would then be external, it can be cooled so as to remove the heat at the point at which it is generated rather than at the substrates. Further, in normal sputtering from a target of approximately the same size as the bell jar, it is generally observed that the glow region does not extend to the edges of the target, but is bonded by an inactive penumbra. Since the same type of behavior would be expected in reactive sputtering, this geometry should eliminate the problems that are presently believed to be due to the target support structure. Completion of this new arrangement awaits delivery of the Si disk. Procuring this disk has been a substantial problem since Si producers apparently have no casting facilities. Hughes Santa Barbara Operation, from whom the disk was finally ordered, is

able to cast Si disks to 12 inch diameter insuring that this geometry could be scaled-up.

While gas composition has little effect on film quality, it does have a pronounced effect on deposition rate. As expected, sputtering in a high percentage of O₂ is much slower than in a high percentage of Ar. While compositions containing as low as 5% O₂ appear to give films of pure SiO₂, most of the experimental work is being done with a 70% Ar-30% O₂ mixture. Contrary to the literature values,^(1,2) IPC has found that, for close (~1 inch) anode-substrate spacings, pressures in the range of 200 micron are desirable. This discrepancy is not presently explainable. Under the normal operating conditions, sputtering current is limited by the power supply. (A larger supply will be used on the new arrangement.) The anode-cathode spacing was chosen empirically to maximize the deposition rate but is probably not optimum.

2.1.2 Electron Beam Evaporation

While the reported deposition rates for electron beam evaporated SiO₂ are ~240 x 10³ Å/hr for a 2 kw gun, 10 inches from the substrates, thick SiO₂ films are not adherent to Si. Samples made by a commercial vendor (Nuclide Corporation) for the proposal for this contract demonstrated both this fact and additionally that splitting occurred when evaporated SiO₂ was deposited over a layer of high vacuum sputtered SiO₂. Since thick evaporated SiO₂ is reportedly adherent to Cu, Al and soda glasses, the latter phenomena is thought to be due to improper cleaning of the sputtered SiO₂ interface prior to SiO₂ evaporation. To eliminate this possibility it was decided that the electron beam gun should be integrated into the sputtering apparatus so that the two layers could be blended together. To this end a small commercial (Varian) gun was ordered and was to be fitted into the small high vacuum sputtering apparatus. Delivery of the gun has, however, been several months longer than was quoted. It is now promised for the last week in September.

As is the case in high vacuum sputtering it is reportedly necessary to employ an O₂ leak in electron beam evaporation of SiO₂ in order to prevent deposition of SiO. With this precaution evaporated SiO₂ layers are reported to be clear and free of absorption in the visible range.

2.2 Other Materials

Lead glass (Corning 8362) films, ~1 x 10³ Å thick, have been high vacuum sputtered onto quartz substrates in the small sputtering apparatus. The poor thermal properties of the lead glass target necessitated operation at very low beam current making deposition of thick films prohibitive. While the films were clear and appear otherwise acceptable, it is likely that cracking of the target when heated is indicative of coverslip cracking during thermal cycling. A longer run will be made with a Si substrate to confirm this point. If, as anticipated, lead glass films do crack, they will not be pursued further.

In work not supported by this contract, MgO, Al₂O₃ and Si₃N₄ (?) layers have been deposited by high vacuum reactive sputtering in the small system. In this technique, a suitable gas leak is used in conjunction with the appropriate metallic target to form the desired compound. Only thin ($\sim 2 \times 10^3$ Å) MgO layers were prepared. Both quartz and GaAs substrates were used. The films on quartz were transparent and showed no absorption. The Al₂O₃ films were deposited on quartz to a thickness of ~ 2 micron. They also showed no absorption in the visible range. The Si₃N₄ (?) films were brownish, however, suggesting SiO contamination. Since no steps to eliminate O₂ from the bleed N₂ were taken, these results were not unexpected. (Essentially, similar behavior was observed in an earlier attempt to deposit Si₃N₄ by conventional reactive sputtering.)

2.3 Thermal Cycling

The contract goals call for 6 mil slipped cells to withstand repeated thermal cycling between -100 and +100°C (see Figure 4). Developmental cells with coverslip thicknesses in the 0.5 to 2.0 mil range have been repeatedly cycled between 77°K and 200°C with no apparent effect. Slipped cells have also been heated to 400°C without deleterious effects. It should be noted, however, that these tests were performed as thermal shock tests as well as temperature cycling tests. While slips in this thickness range are able to survive thermal shock, it is expected that cells with slips thicker than 4 to 5 mils would crack when thermally shocked.

As a consequence of this expectation, a thermal cycling test set is being designed that will provide something approaching the allowed 10 minute transit time between temperature extremes. The test set will consist of a closed box having a multiplicity of interconnected passages in its walls. Hot and cold gases will be alternately cycled through these passages to produce the temperature extremes. Since the thermal mass of the box will be much larger than that of the cells, the latter should remain in thermal equilibrium with the box. Adjustment of the gas flow rates will give convenient adjustment of the rate of temperature change. This setup could also be used for thermal cycling in vacuum, if required at some future date.

2.4 UV and Vacuum Testing

The contract goals are outlined in Table VI. These tests will be combined as a 30-day vacuum UV test at 100°C. (IPC integral coverslip cells have been tested for UV darkening by WPAFB under a cooperative program. The cells were exposed to "1 year" flux with no observable degradation.)

While no UV or vacuum testing has been performed to date, there is little reason to expect difficulties since pure SiO₂ itself does not darken under UV exposure and the slips are deposited in vacuum. The testing will be done in a water cooled 8 inch diameter stainless steel pipe "tee" that is attached to a high-speed 6 inch oil diffusion pumping system. The pumping system includes

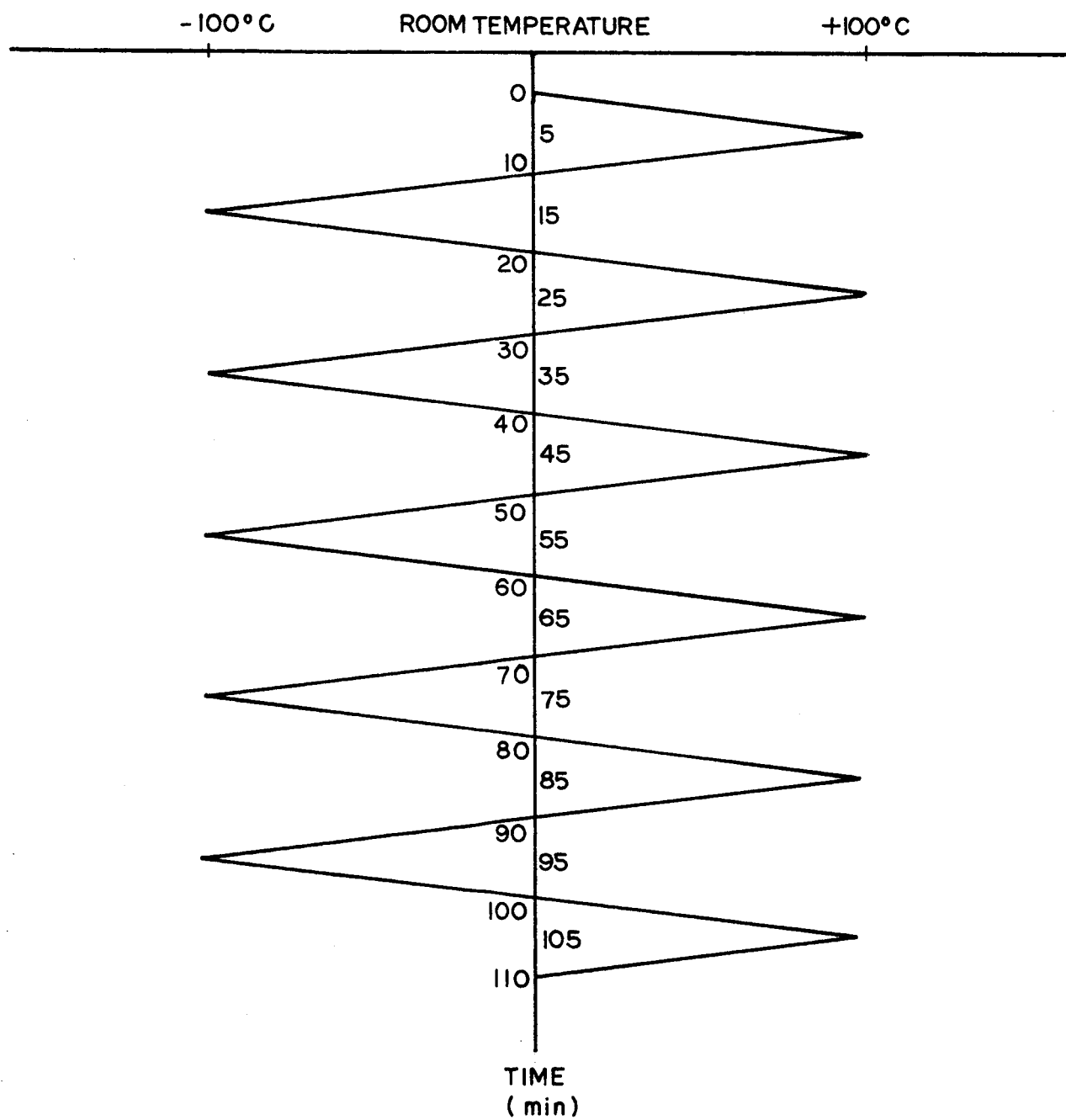


Figure 4. Thermal Cycle Test

Table VI
Environmental Test Specifications
(To be Performed on 6 Mil Thick Coverslips)

Test	Conditions	End Points
Thermal Cycle	-100 to +100°C (see Figure 2)	No physical deterioration
UV Degradation	500 hr at 12.5 mw-cm ²	5% transmission loss between 0.4 and 1.1 microns
Vacuum Storage	30 days at 100°C in 10 ⁻⁶ torr vacuum	No physical deterioration, weight loss or transmission loss
Proton Degradation	0.5 Mev, 10 ¹⁴ -cm ²	5% transmission loss between 0.4 and 1.1 microns
Electron Degradation	1.0 Mev, 10 ¹⁶ -cm ²	5% transmission loss between 0.4 and 1.1 microns

an ambient cooled cold cap, on the pump, and a mechanically refrigerated chevron trap. A 250 watt General Electric UVIARC lamp is being used as the light source. The slipped cells and test depositions will be supported on an electrically heated plate in the center of the vacuum chamber. While some tests will consist of determining the change in transmission of slips deposited on quartz plates, the majority of the tests will be made on slipped cells by comparing their photoresponse before and after exposure.

2.5 Radiation Testing

The contract goals are outlined in Table VI. Since the range of 0.5 Mev protons is considerably less than 6 mils, this testing can be done on slipped cells. To date, no detectable change in cell response has been observed after exposure to 10^{15} protons/cm². Since 10^{16} /cm² 1 Mev electrons will substantially degrade cells protected by 6 mil SiO₂ coverslips, much of the electron testing will have to be done on slips deposited on quartz plates. As a supplement to these tests, slipped cells will be irradiated and analyzed by examining their differential photoresponse. Since irradiation effects on the cell itself will occur in the red end of the spectrum and the slip darkening is expected at the blue end, unchanged blue response would be indicative of undegraded slip transmission.

3. FUTURE PLANS

While the poor deliveries on the electron beam gun and large Si target have set the program back one to two months, the final goals should be relatively unaffected. The choice between reactive sputtering and electron beam evaporation will have to be postponed to the end of the second quarter. No other problems are anticipated.

4. REFERENCES

- (1) Sinclair, W. R. and Peters, F. G., J. Am. Ceram. Soc., 46, 20 (1963).
- (2) Smith, E. E. and Kennedy, D. R., Proc. IEE (London), 109, (Part B, Supp. 22), 504 (1962).

DISTRIBUTION LIST

<u>Addressee</u>	<u>Copies</u>
NASA-Goddard Space Flight Center Greenbelt, Maryland 20771 Attention:	
Office of the Director - Code 100	1
Office of the Assistant Director for Administration and Technical Services - Code 200	3
Office of the Assistant Director for Projects - Code 400	1
Office of the Assistant Director for Systems Reliability - Code 300	1
Office of the Assistant Director for Tracking and Data Systems - Code 500	1
Office of the Assistant Director for Space Sciences - Code 600	1
Office of the Assistant Director for Technology - Code 700	1
GSFC Library - Code 252	2
Contracting Officer - Code 247	1
Technical Information Division - Code 250	4
Technical Representative - Code 716	25
NASA Headquarters FOB 10B Washington, D.C. 20546 Attn: Arvin Smith, Code RNW	1
Anderson, Donald NASA/Ames Research Center Moffett Field, California	1
Bachner, Robert L. Solar Systems, Inc. 8241 N. Kimball Avenue Skokie, Illinois 60078	1

<u>Addressee</u>	<u>Copies</u>
Baicker, J. A. Princeton Research and Development Company Box 641 Princeton, New Jersey	1
Barkley, Dwight W. Liberty Mirror, L. O. F. Brackenridge, Pennsylvania 15014	1
Brancato, E. L. N. R. L. Washington, D. C.	1
Chamberlin, R. R. National Cash Register Company Main and K Streets Dayton, Ohio	1
Cherry, William R. NASA/Goddard Space Flight Center Greenbelt, Maryland 20771	1
Cole, Robert L. Texas Instruments Dallas, Texas	1
Cusano, Dominic A. General Electric, R&D Center P. O. Box 1088 Schenectady, New York	1
Dawson, John R. NASA/Langley Research Center Langley Station Mail Stop 188-B Hampton, Virginia 23365	1
Downing, R. G. TRW Systems 1 Space Park Redondo Beach, California	1
Fang, P. H. (Dr.) NASA/Goddard Space Flight Center Greenbelt, Maryland 20771	1

<u>Addressee</u>	<u>Copies</u>
Ferguson, George D. (Jr.) General Electric Carroll Avenue Lynchburg, Virginia	1
Finger, Harold B NASA Headquarters Washington, D. C. 20546	1
Fischell, Robert JHU/Applied Physics Laboratory Silver Spring, Maryland	1
Hamilton, Robert C. Institute for Defense Analyses 400 Army-Navy Drive Arlington, Virginia 22202	1
Hawkins, Kenneth D. Ryan Aeronautical Company Lindberg Field San Diego, California 92112	1
Haynes, Gilbert A. NASA/Langley Research Center Langley Station Hampton, Virginia 23365	1
Holloway, H. Philco Research Laboratory Blue Bell, Pennsylvania	1
Hood, John Dow Corning Corporation Hemlock, Michigan 48626	1
Iles, Peter A. Hoffman Electronics Corporation 4501 Arden Drive El Monte, California	1
Jilg, Eugene T. Communications Satellite Corporation 2100 L Street, N. W. Washington, D. C. 20037	1

<u>Addressee</u>	<u>Copies</u>
Johnson, Carl E. Bellcomm, Inc. 1100 17th Street, N. W. Washington, D. C.	1
Julius, Richard F. Keltec Industries, Inc. 5901 Edsall Road Alexandria, Virginia 22314	1
Kaye, S. Electro-Optical Systems Inc. 300 No. Halstead Street Pasadena, California	1
King, W. J. (Dr.) Ion Physics Corporation Burlington, Massachusetts 01803	1
Kittl, Emil U. S. Army Electronics Command Attn: AMSEL-KL-PA Fort Monmouth, New Jersey CC-07703	1
Kling, Harry P. Hittman Associates Beltimore, Maryland	1
Loferski, Joseph J. (Dr.) Brown University Providence, Rhode Island	1
Marks, Burton S. Lockheed Missile and Space Company Palo Alto, California	1
Massie, Lowell D. AF Aero Propulsion Laboratory APIP-2 Wright-Patterson Air Force Base, Ohio	1
Mlavsky, A.I. (Dr.) Tyco Laboratories, Inc. Bear Hill Waltham, Massachusetts 02154	1

<u>Addressee</u>	<u>Copies</u>
Mott, James L. Fairchild Hiller Corporation Rockville, Maryland	1
Oman, Henry Boeing Company Seattle, Washington 98166	1
Pearson, Gerald L. Stanford University Stanford, California	1
Potter, Andrew NASA/Lewis Research Center 21000 Brookpark Road Cleveland, Ohio 44135	1
Plauche, Fulton M. NASA/Manned Space Flight Center EP-5 Houston, Texas 77058	1
Ralph, E. L. Heliotek 12500 Gladstone Avenue Sylmar, California	1
Rappaport, Paul RCA Laboratories Princeton, New Jersey	1
Ray, Kenneth A. Hughes Aircraft Company El Segundo, California	1
Reynard, Duncan L. Philco WOL Palo Alto, California	1
Riel, Robert K. Westinghouse Electric Corporation Semiconductor Division Youngwood, Pennsylvania 15697	1

<u>Addressee</u>	<u>Copies</u>
Ritchie, Donald W. Jet Propulsion Laboratory Pasadena, California	1
Schach, Milton NASA/Goddard Space Flight Center Greenbelt, Maryland 20771	1
Schaefer, James C. Harshaw Chemical Company 1945 E. 97th Street Cleveland, Ohio	1
Schlotterbeck, R. S. General Electric Company Lynchburg, Virginia	1
Schwarz, F. C. NASA/ERC 575 Technology Square Cambridge, Massachusetts 02139	1
Shirland, F. A. Clevite Corporation 540 E. 105th Street Cleveland, Ohio 44108	1
Slifer, Luther W. (Jr.) NASA/Goddard Space Flight Center Greenbelt, Maryland	1
Timberlake, Allen B. Battelle Memorial Institute 505 King Avenue Columbus, Ohio 43201	1
Waddel, Ramond C. (Dr.) NASA/Goddard Space Flight Center Greenbelt, Maryland 20771	1
Winkler, Seymour H. RCA/AED P. O. Box 800 Princeton, New Jersey 08540	1

<u>Addressee</u>	<u>Copies</u>
Wise, Joseph F. USAF-APL APIP-2 Wright-Patterson Air Force Base Dayton, Ohio	1
Yannoni, Nicholas F. AF Cambridge Research Laboratories L. G. Hanscom Field Bedford, Massachusetts 01731	1
Wolf, Martin RCA/AED Princeton, New Jersey	1
Marinozzi, D. Optical Coating Laboratories Santa Rosa, California	1
Starkey, Gerald E. (Major) Headquarters USAF AFRSTD Pentagon Washington, D. C.	1
Werth, John J. General Motors Defense Research Laboratories 6767 Hollister Avenue Goleta, California	1